Korean J. Chem. Eng., **20**(3), 415-428 (2003)

FEATURED REVIEW

Chemical Reaction Engineering in the Chemical Processing of Metals and Inorganic Materials

Part II. Chemical Process Modeling and Simulation

Hong Yong Sohn†

Departments of Metallurgical Engineering and of Chemical and Fuels Engineering,
University of Utah, Salt Lake City, Utah 84112, U. S. A.

Abstract–In traditional chemical reaction engineering, it is possible to incorporate only the simplified aspects of fluid flow, mixing, and mass/heat transfer into the analysis of chemical reaction rates and reactor design. As a consequence of the advent of high-speed, high-capacity computing capacity, complex processes involving chemical reactions have become amenable to analysis and modeling. This has also resulted in the merging of various disciplines of chemical engineering in formulating detailed descriptions of complex processes. Developments that exemplify this trend over the years are discussed in this review. Several examples from the author's previous work are used to illustrate the application of chemical reaction engineering principles to the modeling and analysis of complex systems involving the chemical processing of metals and other inorganic materials.

Key words: Chemical Reaction Engineering, Fluidized-bed Reactor, Gas-particle Flow, Liquid-liquid Emulsion, Process Modeling, Solvent Extraction

INTRODUCTION

Complex processes involving chemical reactions have become amenable to analysis and modeling thanks to the rapidly increasing computational capacity. Traditional chemical reaction engineering incorporates only the simplified aspects of fluid flow, mixing, and mass/heat transfer into the analysis of chemical reaction rates and processes. As a result, accurate and realistic analyses and simulations of many individual aspects of complex processes have not been possible. Thus, the disciplines of chemical reaction engineering and transport phenomena have stood separate, and their aspects within a given process were treated individually [Similarly, unit operations and transport phenomena were treated separately]. A consequence of the availability of high-speed, high-capacity computing capacity has been the merging of these disciplines into the formulation of a more detailed description of a complex process. Currently, many models combine the basic principles of various previously independent sub-disciplines of chemical engineering to formulate comprehensive and increasingly more realistic descriptions of chemical processes.

Developments that exemplify this trend over the years in the field of chemical processing of metals and other inorganic materials are discussed in this review. The examples will largely be drawn from the work by the author and his coworkers, because of the limitations in the scope of the review and time available to prepare this article. Regrettably, therefore, excellent examples by many other researchers have to be left out.

FLASH REACTION PROCESSES

An important example of a unit process in metals production is the flash smelting process in the production of nonferrous metals from sulfide minerals. A schematic diagram of this process is given in Fig. 1. In this process, fine, dried mineral particles and fluxes are injected into the furnace with industrial oxygen or oxygen-enriched air. The mineral particles are rapidly ignited and burn in the turbulent gas jet. The flash-smelting process has the advantages of rapid reaction rate, ease of control, substantial reduction in fuel requirements, and efficient sulfur dioxide capture.

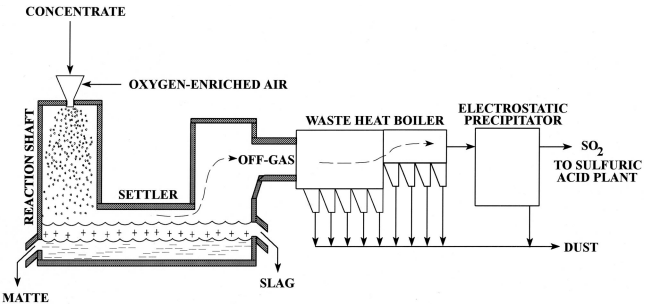

Fig. 1. Schematic diagram of the flash smelting process.

Despite the fact that the process has been in commercial use for a long time and is currently the dominant sulfide-smelting process, the design and operation of a flash-smelting furnace has largely remained an art. This is mainly due to the difficulty of understanding and quantifying the complex interactions of the individual sub-processes involved - the turbulent fluid flow, convective heat and mass transfer, chemical reactions, and radiative heat transfer.

In our research on an experimental and mathematical modeling investigation of the shaft region of a flash-smelting furnace, we began by first tearing apart the overall process into identifiable component processes. We thus recognized a number of important subprocesses, as shown in Fig. 2. The model equations were written based on the continuity of mass and the conservation of momen-

†To whom correspondence should be addressed.
E-mail: hysohn@mines.utah.edu

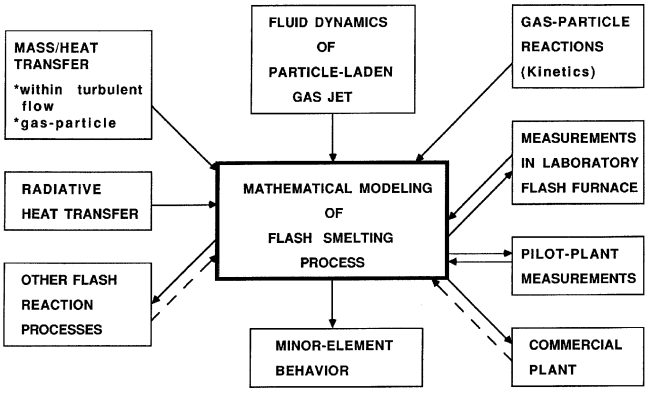

Fig. 2. Components of mathematical modeling of the flash-smelting process.

tum and energy for the gas and the particle phases [Hahn and Sohn, 1990; Perez-Tello et al., 2001]. The gas phase was described from the Eulerian point of view. The time-averaged equations for the conservation of fluid properties can be expressed in the following general form:

$$\nabla\bullet(\rho\vec{v}\phi)-\nabla\bullet(\Gamma_\phi\nabla\phi)=S^\phi \tag{1}$$

where ϕ is the dependent variable, Γ_ϕ is the coefficient for the diffusive transfer, and S^ϕ is the source term. Table 1 shows all the gas-phase governing equations. The standard k-ε model was used to represent gas-phase turbulence. The particle phase was described using the Lagrangian framework, the governing equation being listed in Table 2. Further details of the model equations can be found elsewhere [Hahn and Sohn, 1990; Perez-Tello et al., 2001].

The next sub-process we tackled was the gas-particle reactions - the oxidation of sulfur and iron in the mineral particles. To describe the ignition transient as well as the main combustion period following the ignition, information on the intrinsic kinetics of the mineral particle oxidation is needed. This information was obtained by carrying out separate experiments [Chaubal and Sohn, 1986]. Appropriate measures were taken to ensure determination of the intrinsic kinetics. After the particle becomes molten in the flash furnace, the particle temperature is sufficiently high that the overall rate of reaction can be described by the mass-transfer rate of oxygen from the

Table 1. Gas-phase equations

Equation	$\frac{\partial}{\partial x}(\overline{\rho}_g\overline{u}_g\phi)+\frac{\partial}{\partial y}(\overline{\rho}_g\overline{v}_g\phi)+\frac{\partial}{\partial x}(\overline{\rho}_g\overline{w}_g\phi)-\frac{\partial}{\partial x}\left(\Gamma_\phi\frac{\partial\phi}{\partial x}\right)-\frac{\partial}{\partial y}\left(\Gamma_\phi\frac{\partial\phi}{\partial y}\right)-\frac{\partial}{\partial z}\left(\Gamma_\phi\frac{\partial\phi}{\partial z}\right)=S^\phi$			
	ϕ	Γ_ϕ	S^ϕ	
Continuity	1	0	S_m^p	(A-1)
x-Momentum	$\overline{u}_g$	μ_e	$-\frac{\partial p}{\partial x}+\frac{\partial}{\partial x}\left(\mu_e\frac{\partial\overline{u}_g}{\partial x}\right)+\frac{\partial}{\partial y}\left(\mu_e\frac{\partial\overline{v}_g}{\partial x}\right)+\frac{\partial}{\partial z}\left(\mu_e\frac{\partial\overline{w}_g}{\partial x}\right)-\frac{2}{3}\frac{\partial}{\partial x}(\overline{\rho}_g k)+\overline{\rho}_g g_x+S_p^u$	(A-2)
y-Momentum	$\overline{v}_g$	μ_e	$-\frac{\partial p}{\partial y}+\frac{\partial}{\partial x}\left(\mu_e\frac{\partial\overline{u}_g}{\partial y}\right)+\frac{\partial}{\partial y}\left(\mu_e\frac{\partial\overline{v}_g}{\partial y}\right)+\frac{\partial}{\partial z}\left(\mu_e\frac{\partial\overline{w}_g}{\partial y}\right)-\frac{2}{3}\frac{\partial}{\partial y}(\overline{\rho}_g k)+\overline{\rho}_g g_y+S_p^v$	(A-3)
z-Momentum	$\overline{w}_g$	μ_e	$-\frac{\partial p}{\partial z}+\frac{\partial}{\partial x}\left(\mu_e\frac{\partial\overline{u}_g}{\partial z}\right)+\frac{\partial}{\partial y}\left(\mu_e\frac{\partial\overline{v}_g}{\partial z}\right)+\frac{\partial}{\partial z}\left(\mu_e\frac{\partial\overline{w}_g}{\partial z}\right)-\frac{2}{3}\frac{\partial}{\partial x}(\overline{\rho}_g k)+\overline{\rho}_g g_z+S_p^w$	(A-4)
Turbulent kinetic energy	k	μ_e/σ_k	$G-\overline{\rho}_g\varepsilon$	(A-5)
Dissipation rate	ε	μ_e/σ_ε	$(\varepsilon/k)(C_1G-C_2\overline{\rho}_g\varepsilon)$	(A-6)
Sulfur mass fraction	f	μ_e/σ_f	S_p^f	(A-7)
Reacted oxygen ratio	η	μ_e/σ_η	S_p^η	(A-8)
Enthalpy	$\overline{h}_g$	μ_e/σ_h	$Q_{rp}^h+Q_{rg}^h+\overline{u}_g\frac{\partial p}{\partial x}+\overline{v}_g\frac{\partial p}{\partial y}+\overline{w}_g\frac{\partial p}{\partial z}+S_p^h$	(A-9)

where:

$$G=\mu_t\left\{2\left[\left(\frac{\partial\overline{u}_g}{\partial x}\right)^2+\left(\frac{\partial\overline{v}_g}{\partial y}\right)^2+\left(\frac{\partial\overline{w}_g}{\partial z}\right)^2\right]+\left(\frac{\partial\overline{u}_g}{\partial y}+\frac{\partial\overline{v}_g}{\partial x}\right)^2+\left(\frac{\partial\overline{u}_g}{\partial z}+\frac{\partial\overline{w}_g}{\partial x}\right)^2+\left(\frac{\partial\overline{v}_g}{\partial z}+\frac{\partial\overline{w}_g}{\partial y}\right)^2\right\} \tag{A-10}$$

$$\mu_e=\mu_t+\mu_l \tag{A-11}$$

$$\mu_t=C_\mu\overline{\rho}_g k^2/\varepsilon \tag{A-12}$$

$$S_p^m=S_p^f-S_p^\eta \tag{A-13}$$

Table 2. Particle-phase equations

Motion	$m_p\frac{d\langle\mathbf{V}\rangle}{dt}=m_p\frac{3}{4}C_D\frac{\rho_g}{\rho_p}\frac{1}{d_p}\lvert\langle\mathbf{U}\rangle-\langle\mathbf{V}\rangle\rvert(\langle\mathbf{U}\rangle-\langle\mathbf{V}\rangle)+(m_p-m_g)\mathbf{g}$	(B-1)
Particle dispersion (cloud model)	$\sigma_{ii}^2(t)=2\int_0^t\langle v_i'^2(t_1)\rangle\int_0^t R_{ii}^p(\tau)d\tau dt_1$	(B-2)
Species mass balance	$\frac{dn_i}{dt}=\sum_{j=1}^{j=q}R_{i,j}^r-R_i^v$	(B-3)
Energy	$\frac{d}{dt}(m_ph_p)=H_r+Q_{rp}-Q_p-H_v$	(B-4)

bulk gas.

The ability of the computer model to describe the dispersion of the particles in the turbulent gas jet of a flash-smelting furnace shaft was verified by the use of a non-reacting model system [Yasuda and Sohn, 1995]. This work was done using a room-temperature model apparatus by combining a photographic method and a computer image-analysis technique. The observation chamber was a rectangular box made of acrylic plates and lined with glass plates to prevent the particles from sticking to the wall. The height of the chamber was 1.22 m, and the width and length were both 0.61 m. A steady flow of a gas-particle jet was injected from the center of the ceiling through a variety of injector and withdrawn through an outlet at the bottom of the chamber. Silica sand of 149 to 250 μm was fed through a series combination of a screw feeder and a vibratory feeder to minimize the pulsing of the solid feed. Five 250-W spotlighting halogen lamps were placed on either side of the chamber as the light source, and a black cloth was used for background. The photograph showed the particles as white spots on the black background. A sample of the comparison between the experimental and computed results is shown in Fig. 3. It is noted that the computer model yields the particle number density in the units of number per unit volume, whereas the photographic data gave it as number per unit projected area. Thus, the computed data were converted by integrating through the depth of the system. As can be seen, the agreement is quite satisfactory, thus verifying the validity of the fluid-dynamic description used in the overall computer model from the viewpoint of the particle dispersion in the gas jet.

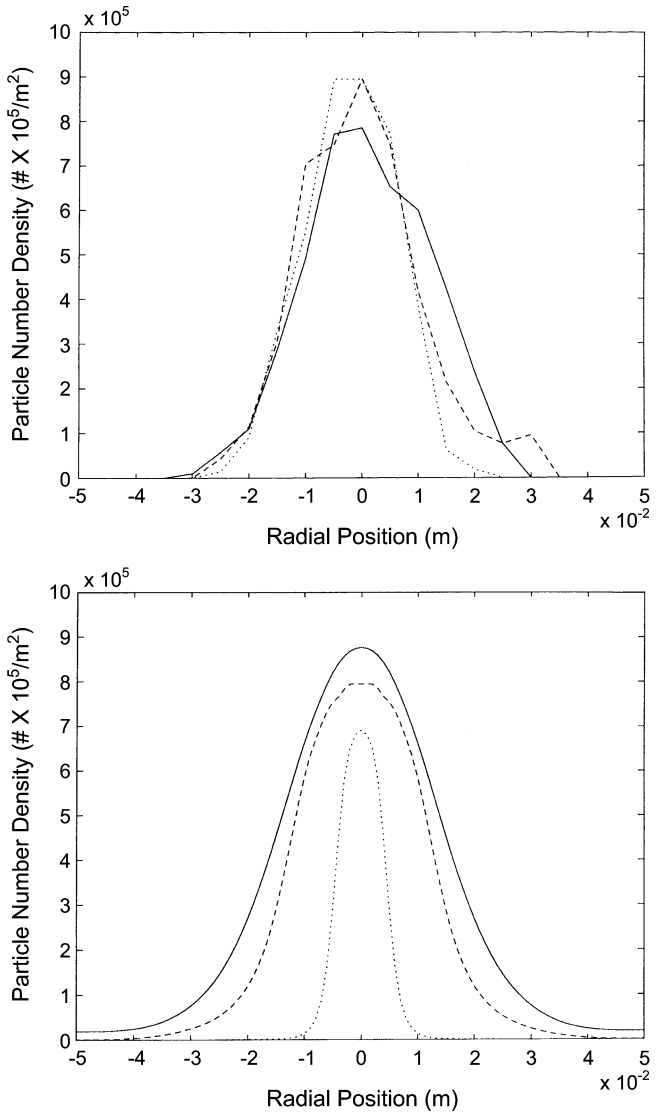

Fig. 3. Comparison between the experimental and computed projected particle number densities in a cold model of flash-furnace shaft: (top) experimental and (bottom) computed (Double-entry injector; 150 mm below the jet entry; air flow rate=0.014 Nm^3/min for primary and 0.084 Nm^3/min for secondary). —— Double-entry injector with 22.0 mm OD inner tube; ····· Double-entry injector with 12.7 mm OD inner tube; ----- Single-entry injector with 25.4 mm ID.

Simultaneously with the mathematical model formulation, we constructed a laboratory flash furnace to make measurements under various operating conditions [Chaubal, 1986; Sohn et al., 1988; Sohn and Seo, 1990; Perez-Tello et al., 2001]. The furnace had an inner diameter of 25 cm and a height of 1.3 m. The maximum solid feeding rate was 5 kg/h. The idea, of course, was to determine how well the mathematical model could predict the experimental measurements and also to use the model to suggest experimental conditions for key measurements. Not satisfied with using just our own data, we obtained data collected independently elsewhere - in this case, measurements obtained in a pilot plant by Outokumpu personnel [Hahn and Sohn, 1990] (Outokumpu, a Finnish company, is a major worldwide licensing company of flash smelting furnaces). In this way, the reliability of the mathematical model could be better established. The mathematical model provides a realistic representation of the process because it is built based on either first principles or well-established correlations for individual sub-processes developed independently. One can thus use the mathematical model with much greater confidence to describe not only the

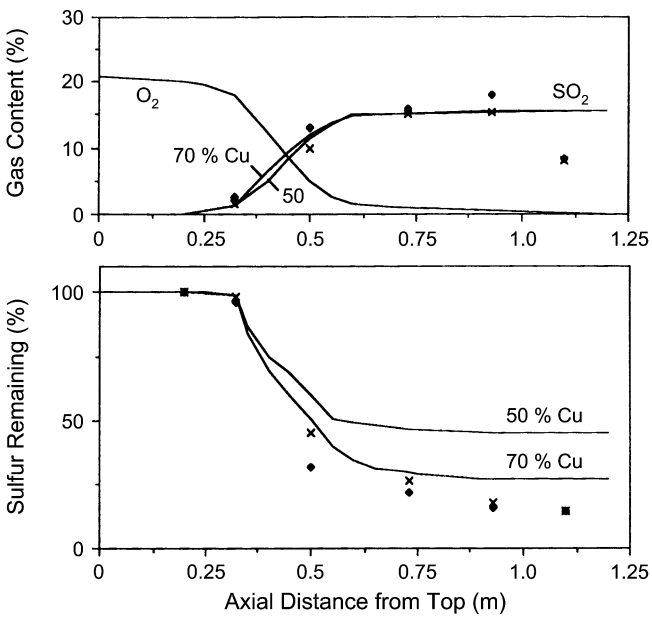

Fig. 4. Comparison of the computed and measured results along the centerline of a laboratory flash furnace shaft [Conditions for the tests are given in Hahn and Sohn, 1990].

sulfide-smelting processes under various operating conditions but also other systems involving a particle-laden gas jet of a similar overall flow configuration. We then applied the computer code to the description of minor-element behavior [Seo and Sohn, 1991], which is an important problem in any smelting process.

Fig. 4 shows a typical comparison between the model predictions and laboratory measurements in terms of the SO_2 concentration in the gas and sulfur content in the particles at various axial positions along the centerline of the furnace shaft [Hahn and Sohn, 1990]. The overall agreement is satisfactory, except near the furnace bottom. The discrepancy toward the bottom of the furnace is due to the air leaking into the furnace through an opening through which the sample probe is inserted. It is particularly noteworthy that the model adequately predicts the particle ignition point, after which the reaction is very fast. A similar comparison between our model predictions and measurements obtained by Outokumpu Co. in their pilot plant is shown in Fig. 5. The top figure shows the SO_2 and O_2 concentrations along the central axis from the burner, as well as the amount of oxygen used in the oxidation of metal contents.

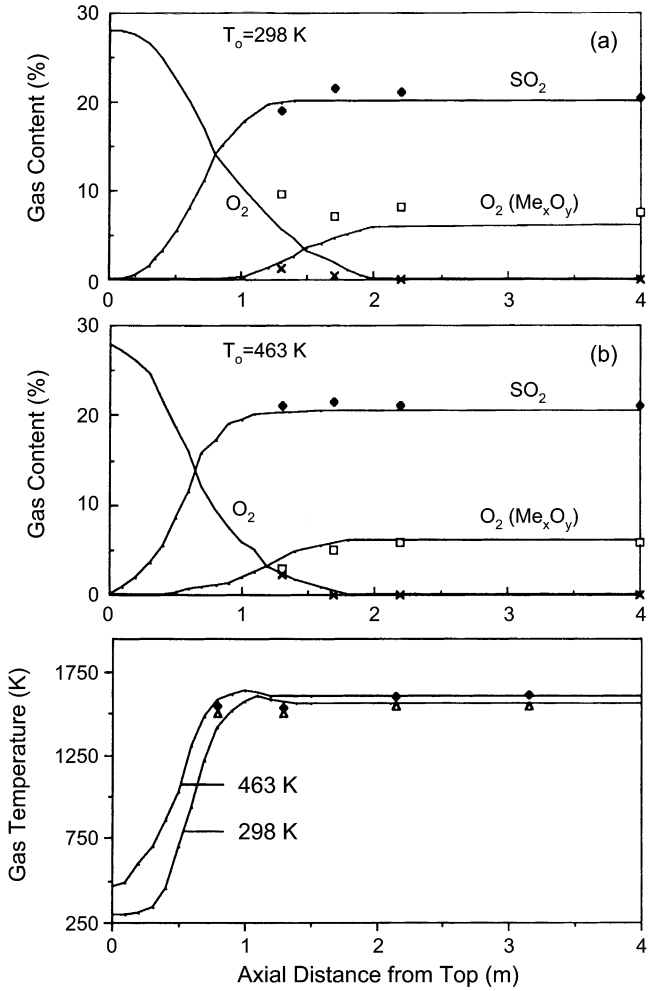

Fig. 5. Comparison of the computed and measured results along the centerline of an Outokumpu pilot flash furnace shaft [O_2 (Me_xO_y) denotes the percent of input O_2 consumed to produce metal oxides. Conditions for the tests are given in Hahn and Sohn, 1990].

The second graph is for the case in which the feed gas was preheated. Considering the complexity of the process and the fact that the pilot-plant measurements were made completely independently from our computation, the agreement is remarkable. The bottom graph compares the temperature profiles for these two cases. Again, the agreement is very good.

Based on the confidence obtained by the good agreement obtained between the model predictions and many other experimental results obtained in our laboratory, the computer model was used to analyze the operation of an industrial flash smelting furnace [Hahn and Sohn, 1990; Perez-Tello et al., 2001; Itagaki et al., 2002]. The most notable aspects of the predictions for a flash-smelting furnace are:

(1) By giving a radial velocity component to the solid particles at the burner tip, particle dispersion becomes more uniform in the furnace, and thus a larger portion of the furnace volume can be utilized for smelting. This is consistent with the new burner developed by Outokumpu Co.

(2) The oxidation reaction is essentially completed within a fraction of the total height typically used for most commercial units. There are a number of reasons why the furnace height cannot be as short as what the calculated result would indicate, such as less reactive recycle materials and agglomeration of the feed concentrate. However, the heights of industrial flash furnaces may, in general, be excessive. In fact, the fact that the height of a commercial furnace can be substantially reduced has been demonstrated by the Hidalgo Smelter of Phelps-Dodge Company (Playas, New Mexico). They removed the top 3 m out of the original 13.5 m from their furnace without any undesirable effects. The associated benefits, including reduced heat loss and refractory requirement, need no further mention.

(3) A large number of "test runs" can be made with the computer simulation without the highly expensive and time-consuming plant tests.

NOVEL SOLVENT EXTRACTION PROCESS

Large operations exist in the chemical and metallurgical industries in which solvent extraction is used to separate, purify, and concentrate values in aqueous solutions [Lo et al., 1983; Alegret, 1988; Jackson, 1986; Blumberg, 1988; Ricci, 1980]. The application of solvent extraction to metal extraction started from the separation of uranium from its ore [Ricci, 1980] and the treatment of spent reactor fuel to separate plutonium from uranium and its fission products [Ricci, 1980; Stoller and Richards, 1961]. Since then, the use of solvent extraction grew rapidly [Lo et al., 1983; Alegret, 1988; Jackson, 1986; Blumberg, 1988]. Two characteristics of the solvent extraction process make it an attractive method for purifying and concentrating solutes dissolved in a solvent: Firstly, solutes can be selectively removed and secondly, they can be concentrated from a dilute solution. Most solvent extraction processes for metal extraction use mixer-settler contactors [Lo et al., 1983; Jackson, 1986]. In the nuclear industry, the most often used contactors are the pulse columns and the mixer-settlers [Extraction '84, 1984], but more recently the centrifugal extractors have become popular for certain applications [Schulte, 1998].

Ideally, the contactor must be simple with few, if any, moving parts. The simplest of these is the spray column in which the heavy and the light phases flow counter-currently in a vertical vessel. Either one of the phases can be the continuous phase with the other being the dispersed phase. Although these types of contactors have the advantages of simple structure with no moving parts, they suffer from relatively low throughput rates (due to their dependence on the small density difference between the two liquid phases) and, most importantly, from severe backmixing which greatly reduces the extraction efficiency and thus necessitates large heights.

The mixer-settler equipment, on the other hand, can be operated under conditions wherein near equilibrium between the two phases is assured. However, it has the disadvantages of considerable complexity of construction and operation due to the requirement of impellers for stirring, interstage pumping, and piping. Furthermore, cleaning and maintenance are quite difficult, especially when corrosive and/or particle-laden liquids are processed [Schulte, 1998; Laddha and Degaleesan, 1978].

Centrifugal extractors are compact and provide good contact between the two immiscible liquids, but have highly complex structure and configurations. For this reason, their operation is difficult and costly. They also provide relatively short contact time and thus are not suitable for solvent extraction systems that have slow kinetics. Other types of contactors that are in use all have internal structures that add varying degrees of complexity and limit the throughput rate per unit volume of the equipment.

A novel solvent extraction process, which overcomes the disadvantages of the existing processes described above, has been developed in the author's laboratory [Sohn and Doungdeethaveeratana, 1998]. The process is carried out in a horizontal countercurrent contactor, in which the liquid-liquid emulsion is generated by a series of bottom-blown gas jets, as shown in Fig. 6. The gas jet creates a plume zone consisting of an emulsion of the two liquids that contains a large interfacial area for rapid mass transfer. The two liquids then disengage and flow in the opposite directions before entering another plume zone. Since the agitation of the two phases and the formation of the emulsion are caused by gas jets, this contactor has no mechanical moving parts and few internal accessories. Thus, the process combines the simplicity of a cylindrical vessel having no moving parts with the contacting efficiency of a mixer-settler as shown below. The equipment is inexpensive to build and operate, and is easy to clean. An important additional advantage of this contactor over mixer-settler equipment is the fact that all the gas can be recirculated, which eliminates solvent loss by evaporation and also prevents mist problems, both of which cause environmental pollution in addition to the loss of process materials. Furthermore, any desired gas atmosphere can be maintained in this system, depending on the required extraction chemistry. The agitation by a gas jet provides a milder and more uniform shear than by a mechanical agitator, and thus generates more uniform droplets [Zaidi and Sohn, 1995] (with fewer very small ones) that coalesce more easily in the phase disengagement zone between the plumes. This will also reduce the problem of crud (third phase) formation, which plagues many solvent extraction operations.

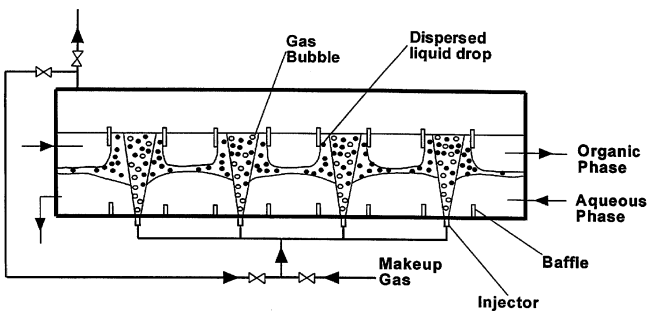

Fig. 6. Schematic diagram of the novel solvent extraction process.

1. Results of Continuous Extraction Test

The performance of the new extraction process has been tested in an apparatus illustrated in Fig. 6 comprising a horizontal clear plastic vessel with 21 holes along the bottom at 10-cm intervals to accommodate gas injection at variable intervals [Sohn and Doungdeethaveeratana, 1998]. The vessel had a circular cross-section and the dimensions of 28.3 cm diameter and 2.4 m length. For a continuous countercurrent extraction test, four injectors at 40 cm intervals were used. The heavy phase was an aqueous solution of copper with an initial concentration of 512 ml/L and pH of 2.15. The light phase was a high-flash-point kerosene containing 2 wt% LIX 860. LIX 860 is one of a number of copper extractants that are commercially available. The diameter of the injectors was 0.56 cm, and the gas velocity at the injector tip was 39 m/s. The flow rate of the organic phase as well as that of the aqueous phase in the vessel was 0.25 L/min. The depth of each phase was 3.8 cm.

A typical example of the test results is plotted as the middle line in Fig. 7 relative to the equilibrium isotherm. The solution concentrations were measured as the liquids left the mixing zones. The initial copper concentration was reduced from 512 mg/L to about 4 mg/L. The efficiency of the mass transfer in the plume generated by the bottom gas injection is seen to be excellent [The reason why the experimental points taken inside the vessel are not on the operating line is mainly because of the complex nature of the flow pattern, which makes it difficult to take samples with the average concen-

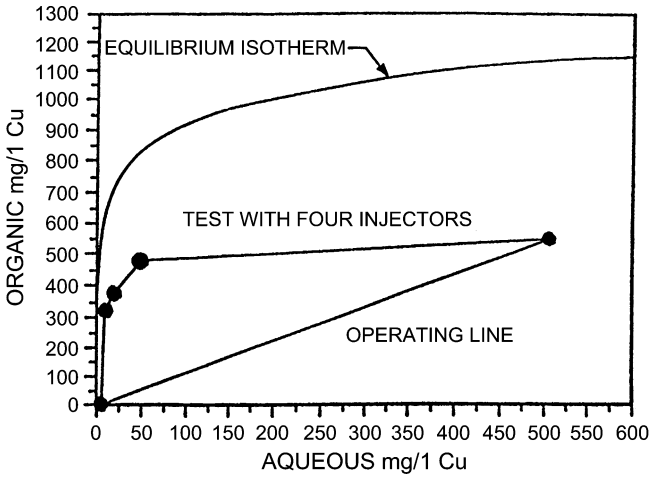

Fig. 7. Result of continuous countercurrent solvent extraction test (The points on the middle curve, from right to left, represent the copper concentration in the aqueous phase vs. that in the organic phase before plume 1, between plumes 1 and 2, etc., up to the region after plume 4).

trations in the particular regions. The copper concentration in the final exit aqueous stream gives the correct final degree of extraction.].

2. Interfacial Area

In order for the process to be industrially feasible, the emulsion generated by the bottom-injected gas jet must have a sufficient interfacial area so that the mass transfer rate may be reasonably rapid. The interfacial area between the two liquid phases in an emulsion generated by bottom gas injection can be estimated using the results of previous work on the drop-size distribution [Zaidi and Sohn, 1995] and the dispersed-phase holdup [Lee and Sohn, 1996] in such emulsions. As discussed below, it has been shown in this work that sufficient interfacial area between the organic and aqueous phases can be generated by bottom gas injection. Furthermore, the interfacial area as well as the drop-size distribution can be controlled by a judicious selection of the gas flow rate and equipment design factors.

The interfacial area per unit volume of the emulsion a is related to the mean drop size and the volume fraction of the dispersed phase ϕ by the following equation [Zaidi and Sohn, 1995; Lee and Sohn, 1996]:

$$a = \frac{A}{V_e} = \frac{6\langle\phi\rangle}{d_{32}}. \quad (2)$$

Here, d_{32} is the Sauter mean diameter of the drops, which is the diameter of the drop having the same volume-to-surface-area ratio as the ratio of the sum of the volumes of all drops to the sum of the surface areas of all the drops.

The Sauter mean diameters of water droplets in kerosene in a bottom-gas-injected liquid-liquid system were measured and correlated with operating conditions [Zaidi and Sohn, 1995]. The experiments were carried out in a 1.5 m long, 0.76 m wide, and 0.76 m high Plexiglas tank. The tank had holes on the bottom to accommodate injectors. Compressed air was injected into the tank containing water and kerosene to form the emulsion. Water was the dispersed phase in this system.

A large specific interfacial area provides a rapid mass transfer rate. On the other hand, the formation of small droplets needs to be avoided because they cause a difficulty with respect to settling and phase disengagement [Nyman et al., 1995]. Therefore, the proper control of drop-size distribution and specific interfacial area is important. The values of d_{32} and a obtained in this work are compared in Table 3 with those for other solvent extraction systems reported in the literature. It is seen that bottom gas injection can generate emulsions with a wide range of specific interfacial areas, including those typical of mixer-settler operations.

3. Degree of Backmixing and the Residence-Time-Distribution Analysis

As mentioned above, an efficient solvent extraction process requires minimum backmixing of each liquid phase in the direction of its overall flow. For counter-currently flowing immiscible liquids in a channel reactor with bottom gas injection at certain intervals, identical to the solvent extraction process described in this article, Iyer and Sohn [Iyer and Sohn, 1994] carried out a dispersion analysis to compare the degree of backmixing in such a system with that in continuous stirred tank reactors in series, much like in mixer-settlers. The degree of backmixing in a channel reactor was expressed by the spread in the measured exit-age distribution curves for a vessel that is identical to that used for the continuous extraction test described earlier [Iyer and Sohn, 1994]. They determined that the new solvent extraction process with just four to six injectors is expected to behave like ten or more mixer-settlers in series, depending on the gas injection conditions, as far as the degree of backmixing is concerned. With a longer channel reactor and more gas injectors, the degree of backmixing can further be reduced. The backmixing and flow characteristics in a countercurrent channel reactor were further determined in a much larger apparatus with 1 m diameter and 7.2 m length. The resident-time distribution and mixing characteristics in this larger unit were well correlated with the equations developed in the smaller unit [Iyer and Sohn, 1994]. Based on this observed flow behavior, extraction efficiencies in the larger unit are expected to be in a similar range to those in the smaller unit.

The overall fluid flow and mixing phenomena in such a channel reactor were investigated, and its residence-time distribution (RTD) was analyzed based on an ideal-reactor-network model [Iyer and Sohn, 1994]. This model is based on the observed flow patterns of the various liquid phases with high-strength bottom gas injection, as shown schematically in Fig. 8 around an injector. In this model, the plume region above an injector was modeled as a continuous stirred tank reactor (CSTR). Since the gas is injected with high energy and the bath is rather shallow, the fluids in the plume region are very well mixed as in a CSTR. Observation of the fluid flow around each plume indicated that a recirculating flow is set up on either side of the plume [Iyer and Sohn, 1994]. Thus, these regions were modeled as recycle plug-flow reactors. A schematic diagram of the combination of ideal reactors used to model the region around each plume, including the plume itself, is shown in Fig. 8. The recycle reactors were assumed to equally share the distance between the two plumes.

Table 3. Comparison of d_{32} and a from this study with those for other solvent extraction systems

Apparatus	d_{32} (mm)	Hold-up (-)	a (m^{-1})	Refs.
Bottom gas injection	4-6	0.03-0.4	40-1,500	Sohn and Doungdeethaveeratana, 1998
Pulsed columns (with sieves or packed)	1-3	0.1-0.4	200-2,400*	Garg and Pratt, 1983; Schmidt, 1983; Simons, 1983; Rauscher and Blass, 1992; Batey et al., 1983
			100-300	Simons and Nap, 1983
Rotating disk or impeller column	1-4	0.1-0.2	150-1,200*	Zhu et al., 1983; Fei and Slater, 1983; Lee and Kim, 1992
Mechanically agitated tank	1-3		600-2,000*	Husung et al., 1983; Laddha and Degaleesan, 1983

*Calculated based on drop size and holdup given in the listed references. When the holdup value was not given, a typical value of 0.3 was assumed.

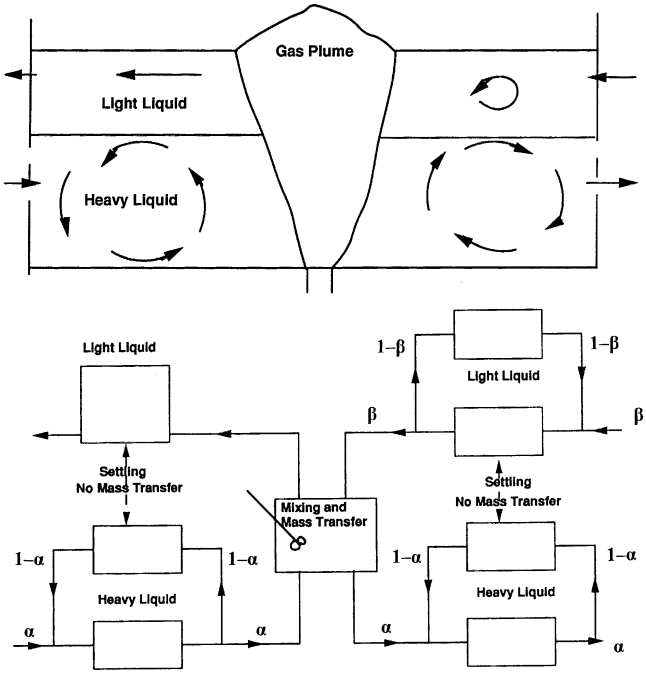

Fig. 8. Flow configuration and ideal-reactor-network model of the bottom-gas-injected solvent extraction process.

The model has a single unknown parameter, α (Fig. 8), the throughput fraction through the combined recycle reactor section. This parameter was determined from the experimental RTD results and correlated against operating variables. All other model variables are determined as functions of α and the known operating conditions.

The model equations are based on the RTD response of the individual ideal reactors. The RTD response E(t) of a plug-flow reactor (PFR) to a pulse input can be written as

$$E(t)=\delta(t-\tau_P). \tag{3}$$

where δ is the Dirac delta function and τ_P is the mean residence time of the PFR.

The CSTR response to a similar pulse input is

$$E(t)=\tau_C^{-1}\exp\left(-\frac{t}{\tau_C}\right) \tag{4}$$

where τ_C is the mean residence time of the CSTR, and the RTD response for the recycle reactor in the heavy phase is

$$E(t)=\alpha(1-\alpha)^n\{\delta[t-\tau_P-n(\tau_P+\tau_R)]\} \tag{5}$$

where τ_R is the mean residence time of the top recycle reactor, and $n=\text{integer}\left[\frac{t-\tau_P}{\tau_P+\tau_R}\right]$.

Considering a CSTR with a normalized input function Y(t) such that

$$\int_{t=0}^{\infty} Y(t)dt=1, \tag{6}$$

the RTD response to the input function introduced between time 0 and $d\theta$ is given by

$$\delta E=\tau_C^{-1}[Y(0)\ d\theta]\exp\left(-\frac{t}{\tau_C}\right). \tag{7}$$

The RTD response to the input function introduced between any time θ and $\theta+d\theta$ is represented by

$$\delta E=\tau_C^{-1}[Y(\theta)\ d\theta]\exp\left[-\frac{t-\theta}{\tau_C}\right]. \tag{8}$$

Therefore, the RTD at any time t is given by

$$E(t)=\int_{\theta=0}^{t}\tau_C^{-1}Y(\theta)e^{-\frac{t-\theta}{\tau_C}}d\theta. \tag{9}$$

The model equations for the various combinations of ideal reactors can be obtained by combining the responses of the individual reactors. The RTD of the first recycle reactor unit and CSTR combination can be expressed as follows:

$$E_1(t)=\sum_{i=1}^{n}\left\{\alpha(1-\alpha)^{n-1}\left[\int_{\theta=0}^{t-\tau}e^{-\tau_{P1}}\tau_{C_1}^{-1}Y(\theta)e^{-\frac{t-\tau-\theta}{\tau_{C_1}}}d\theta\right]\right\} \tag{10}$$

where $\tau=(2i+1)\tau_{P1}$ and $n=\text{integer}\left[\frac{t-\tau_{P1}}{2\tau_{P1}}\right]$, assuming $\tau_P=\tau_R$ [Iyer and Sohn, 1994], while that for the recycle section following the CSTR can be written as

$$E_2(t)=\sum_{i=1}^{n}\alpha(1-\alpha)^{n-1}[E_1(t-\tau)] \tag{11}$$

where $\tau=\tau_{P1}+(2i+1)\tau_{P2}$ and $n=\text{integer}\left[\frac{t-\tau_{P1}-\tau_{P2}}{2\tau_{P1}}\right]$.

These equations can be extended similarly to further identical sections down the length of the reactor by using the response of the previous section as the input function to the next section.

The value of α was determined as the value that gives the best match between the experimental and calculated values for the peak time and the average residence time (the lowest combined difference). A comparison of experimental results with model predic-

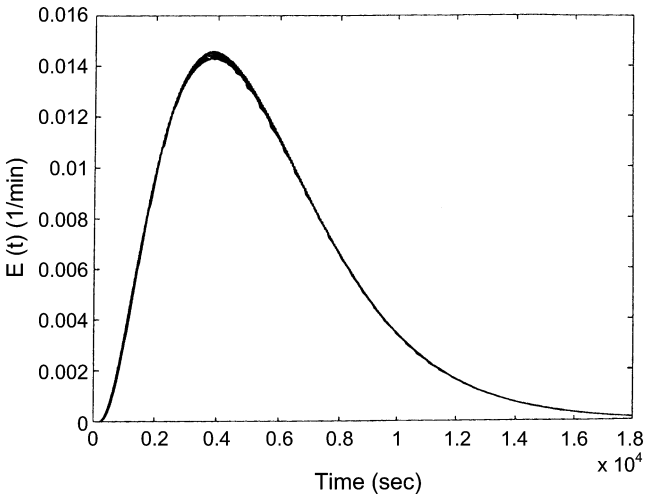

Fig. 9. Computed and experimental residence time distribution in the heavy phase of the bottom-gas-injected countercurrent liquid-liquid process [α=0.025. Detailed test conditions are given in Iyer and Sohn, 1994].

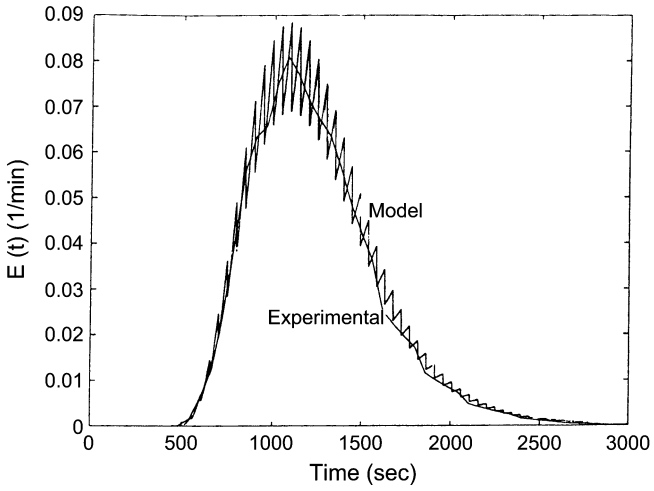

Fig. 10. Computed and experimental residence time distribution in the heavy phase of the bottom-gas-injected countercurrent liquid-liquid process [α=0.225. Detailed test conditions are given in Iyer and Sohn, 1994].

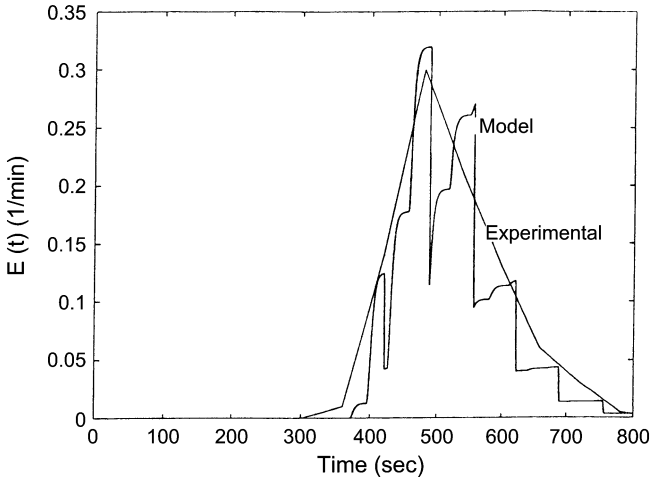

Fig. 11. Computed and experimental residence time distribution in the heavy phase of the bottom-gas-injected countercurrent liquid-liquid process [α=0.644. Detailed test conditions are given in Iyer and Sohn, 1994].

tions of heavy-liquid RTD behavior for three different cases is shown in Figs. 9 through 11. It can be seen that there is an overall excellent fit between the predicted and the experimental RTD curves. The fluctuation in the E(t) value is due to the response characteristics of the idealized recycle reactor unit. The recycle reactor output consists of pulses at intervals of ($\tau_P+\tau_R$) (assumed equal in this work [Iyer and Sohn, 1994]) entering the CSTR. When the CSTR's nominal residence time is small (large α), the magnitude of the fluctuation becomes large. Even for the largest value of α, the time for the peak and the average residence time are represented satisfactorily. Fig. 12 presents the correlation for α against the experimental conditions represented by ε formulated by a dimensional analysis:

$$\varepsilon=\left(\frac{\rho_1 Q_{L1}}{\rho_g Q_g}\right)\left(\frac{h_1}{L}\right)\left[1+\frac{h_2\rho_2}{h_1\rho_1}\right]\left(\frac{\pi d_{inj}^2}{4A_1}\right)^2. \quad (12)$$

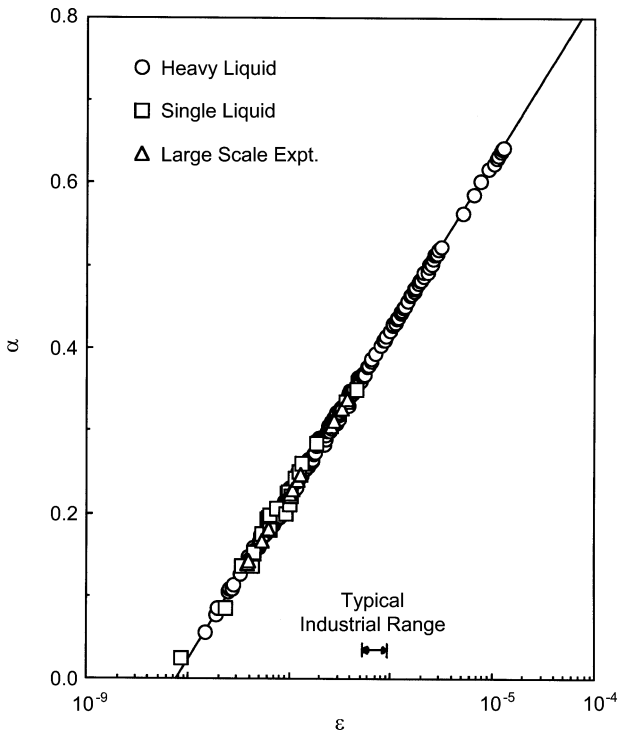

Fig. 12. Variation of α with ε in the heavy phase of the bottom-gas-injected countercurrent liquid-liquid process.

where ρ is the density, Q is the volumetric flow rate, h is the liquid depth, L is the distance between the adjacent gas injectors, A is the cross-sectional area perpendicular to the overall liquid flow, and the subscripts 1 and 2 represent, respectively, the heavy and the light liquid phases.

For the light phase, the model equations are similar to those for the heavy-liquid calculations. The response of the first recycle reactor and CSTR combination is identical to Eq. (10). For the PFR unit downstream of the CSTR, the RTD response is given by

$$\begin{aligned} E_2(t)&=0 \quad \text{for } 0<t<\tau_{P1} \\ &=E_1(t-\tau_{P2}) \quad \text{for } t>\tau_{P2} \end{aligned} \quad (13)$$

These equations can also be extended, as in the heavy-liquid case, to additional identical sections throughout the length of the reactor by using the response of the previous section as the input function to the next section. A comparison of model predictions with experimental results for the light-phase is shown in Fig. 13.

The correlation for the parameter β for the recycling zone of the light phase is given in Fig. 14. The operating conditions are represented, based on a dimensional analysis, by a single dimensionless group γ defined by

$$\gamma=\frac{\rho_2 Q_{L2}}{\rho_g Q_g}\frac{h_1}{L}\left[1+\frac{h_2\rho_2}{h_1\rho_1}\right]\left(\frac{\pi d_{inj}^2}{4A_2}\right)^2. \quad (14)$$

The correlation for α was applied to operations in a much larger vessel (1 m diameter and 7.2 m length) to test its suitability for scale-up. A comparison between the experimental result and the model prediction is shown in Fig. 15, which shows an excellent agreement. The large-scale test for the light phase was not performed because of the limitations on handling a large quantity of hazardous chemicals.

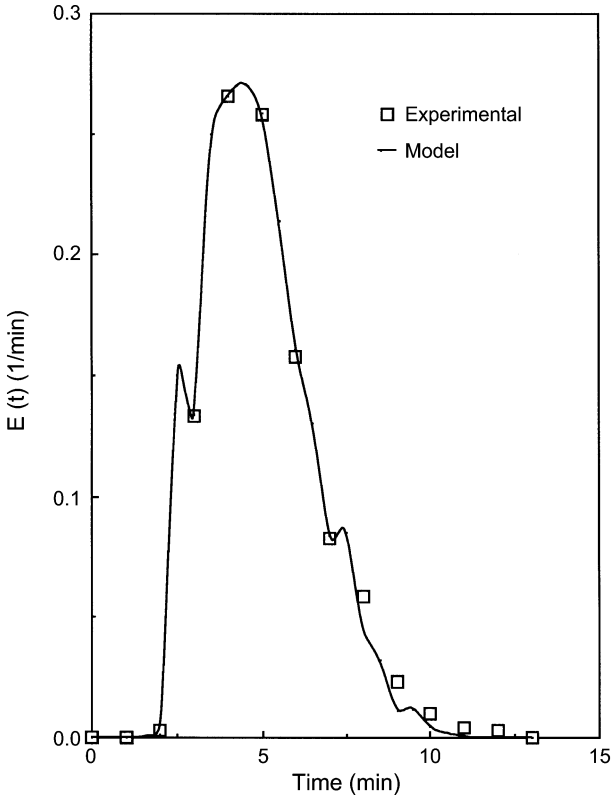

Fig. 13. Computed and experimental residence time distribution in the light phase of the bottom-gas-injected countercurrent liquid-liquid process [β=0.601. Detailed test conditions are given in Iyer and Sohn, 1994].

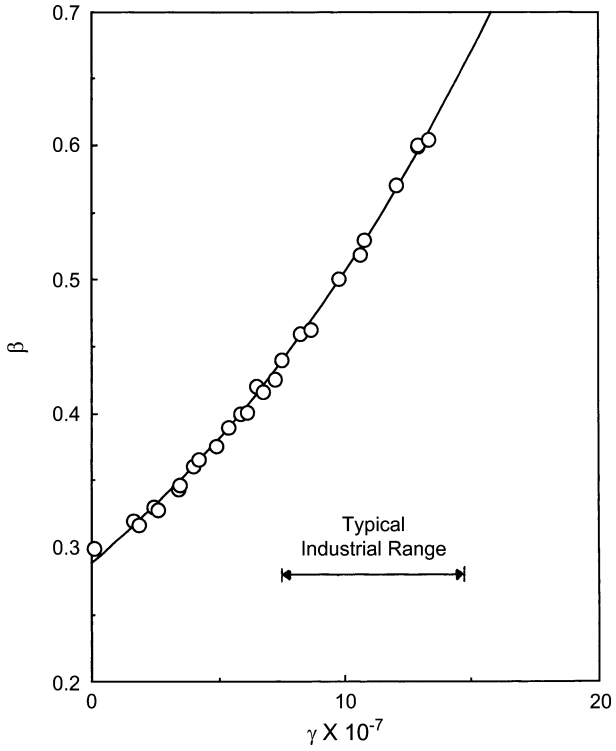

Fig. 14. Variation of β with γ in the light phase of the bottom-gas-injected countercurrent liquid-liquid process.

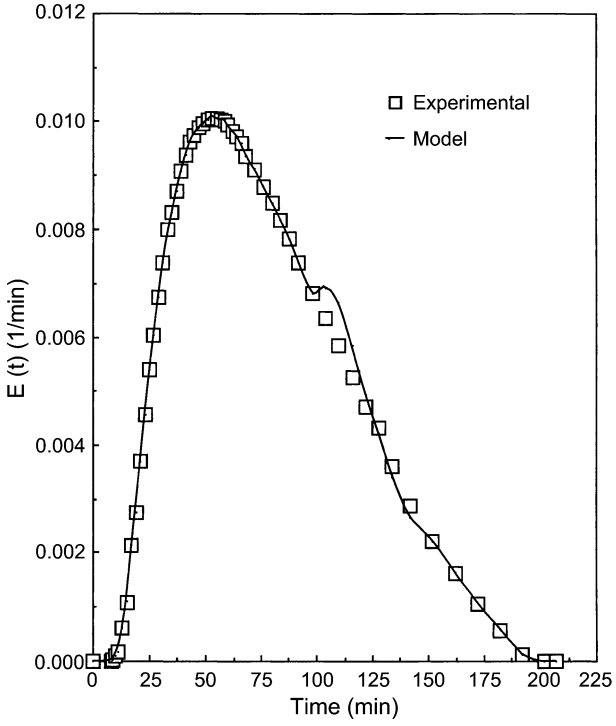

Fig. 15. Computed and experimental residence time distribution in the heavy phase of a large-scale model of the bottom-gas-injected countercurrent liquid-liquid process [α=0.181. Detailed test conditions are given in Iyer and Sohn, 1994].

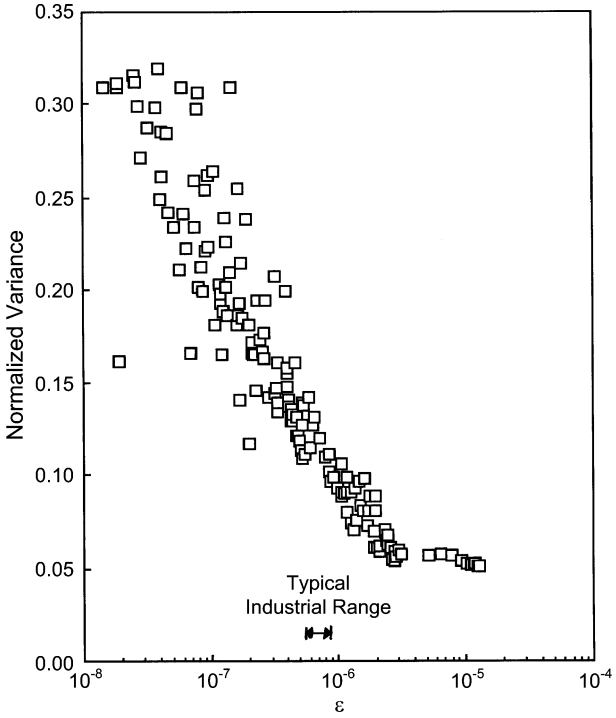

Fig. 16. Variation of normalized variance σ_θ^2 with ε in the heavy phase of the bottom-gas-injected countercurrent liquid-liquid process.

The residence-time distribution represents the degree of back-mixing of fluid elements as they flow through a vessel. The degree

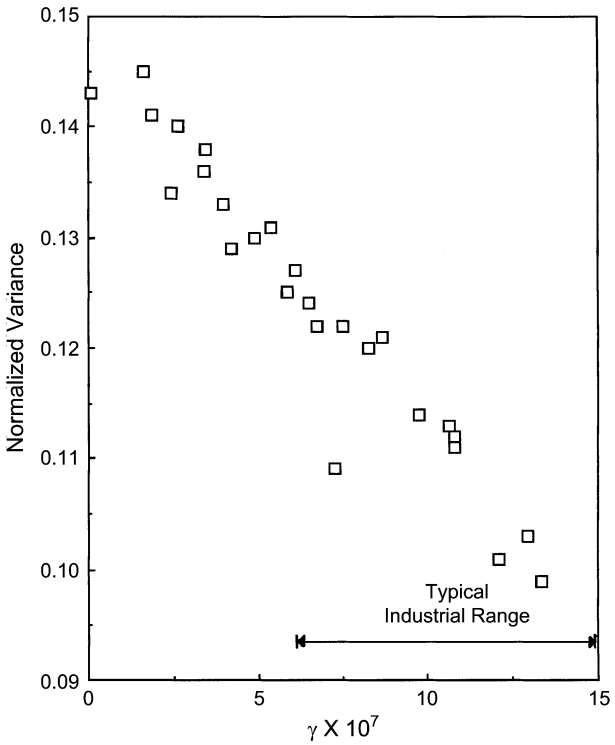

Fig. 17. Variation of normalized variance σ_θ^2 with γ in the light phase of the bottom-gas-injected countercurrent liquid-liquid process.

of backmixing can be represented by the normalized variance $\sigma_\theta^2 = \sigma^2/\bar{t}^2$ of the residence-time distribution [Levenspiel, 1999]. Iyer and Sohn [1994] developed correlations for σ_θ^2 for the heavy and light phases of the bottom-gas-injected counter-flow system against the dimensionless groups ε and γ, respectively, as shown in Figs. 16 and 17. The range of σ_θ^2 between 0.05 and 0.3 for the heavy phase corresponds to the degree of backmixing for 3 to 20 CSTR's in series. The σ_θ^2 values ranging from 0.1 to 0.15 for the light phase are equivalent to the degree of backmixing in 5 to 11 CSTR's in series. This is quite comparable to the mixer-settler systems commonly used in metallurgical solvent extraction, in which a mixer cell is equivalent to a CSTR.

This work has shown how a judiciously constructed network of ideal reactors can be used to represent the residence time distribution of a system in which rather complex flows of liquids take place. The ideal-reactor-network model discussed here further enables one to analyze and predict the rate of mass exchange between the two liquid phases by mass transfer and chemical reaction when combined with the emulsion characteristics discussed earlier and the mass transfer characteristics in such liquid-liquid emulsions [Iyer and Sohn, 1993].

FLUIDIZED-BED REACTOR MODELING FOR GAS-SOLID REACTIONS

Many fluidized-bed processes for non-catalytic gas-solid reactions are operated in the bubbling fluidization mode. Numerous investigations have been carried out to elucidate the phenomena occurring in a bubbling gas-fluidized bed, and many models have been proposed to describe the gas and solid behaviors. The most widely accepted model is the two-phase model [Kato and Wen, 1969; Pyle, 1972; Werther, 1978], in which a fluidized bed is pictured as consisting of a bubble phase that forms from the excess gas flow above the minimum fluidization velocity and an emulsion phase that is similar to the bed in incipient fluidization [Davidson et al., 1997]. A number of different versions of the two-phase model have been proposed. Among them, the Kunii-Levenspiel model [Kunii and Levenspiel, 1991] incorporating the Davidson bubble and wake [Clift and Clift, 1985] is most widely used. Along with the movement of gas in the fluidized bed, the solid particles are dragged upward as clouds or wakes by the bubbles and descend by gravity in the emulsion phase. Fresh particles may be fed continuously to the bed and discharged either through an overflow pipe or by entrainment of gases. Particle size and density may change in a non-catalytic reaction, and particles of the same size have different residence time in the bed. The elutriation rate depends on particle size. All of these must be accounted for in order to predict and control the behavior of the solids in such a fluidized bed process.

Zhou and Sohn [1996] used the bubble assemblage model to describe the bed behavior with several new features. A particle-size-dependent reaction-rate expression, which takes into account the particle-size distribution of the solid, was incorporated to calculate the concentration profile of reactant gases in the bed. This rate expression is more realistic than those previously used [Fuwa et al., 1978; Youn and Park, 1989]. The particle-size distribution in the bed was calculated by a population balance. The model assumes that the solid particles are well mixed throughout the bed, but the gas concentrations vary with the bed height. This makes the model applicable to industrial application where the concentrations of reactant gases may change substantially along the bed height. This model was applied to the analysis of the fluidized-bed chlorination of rutile,

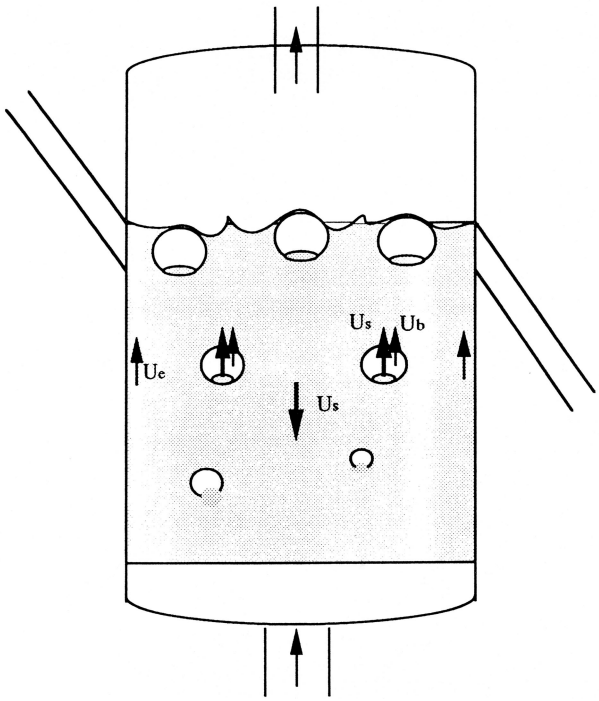

Fig. 18. A schematic representation of the bubbling fluidized bed.

incorporating the experimentally determined intrinsic chlorination kinetics.

With reference to the schematic representation of a fluidized bed shown in Fig. 18, the specific features of the model are:

(1) The bed consists of three regions: bubble, cloud, and emulsion. The gases are exchanged between these regions. Considering other uncertainties in the fluidized-bed model, such as the estimation of gas-interchange parameter and chemical kinetics, the description of the fluidized bed was simplified by neglecting the mass-transfer resistance between the bubble and cloud phases and considering the cloud as part of the bubble phase. The exchange of gaseous species was accordingly simplified to be between the bubble and the dense phases, as has been done before [Youn and Park, 1989; Drinkenburg and Rietema, 1972; Burkur et al., 1974; Rhee and Sohn, 1990].

(2) Fresh rutile particles are fed continuously and mixed with existing particles instantaneously. They react with the gases while being dragged up by the bubbles and descending in the emulsion, and leave the bed either through an overflow pipe or by elutriation.

(3) The gas compositions in the bubble and emulsion phases change with bed height, but the solids are assumed uniformly mixed throughout the bed.

(4) The horizontal variation of gas concentrations in each phase can be neglected.

(5) The bed is operated under an isothermal condition due to the rapid mixing in the bed.

The gases flow through the bubble and emulsion phases, while exchanging mass between the phases. The gas-phase mass balances in these two phases can be expressed as follows:

$$-f_{g,b}U_b\frac{dC_{Ab}}{dZ}=\delta K_{be}(C_{Ab}-C_{Ae})+f_{g,b}(-r_{g,b}) \tag{15}$$

$$-f_{g,e}U_e\frac{dC_{Ae}}{dZ}=\delta K_{be}(C_{Ae}-C_{Ab})+f_{g,e}(-r_{g,e}) \tag{16}$$

where $f_{g,j}$ is the fraction of the bed volume occupied by gas in phase j; K_{be} is the interchange coefficient for gas between the bubble and the emulsion phases based on the bubble volume; and $r_{i,j}$ is the consumption rate of reactant gas i per unit volume of the fluidized bed at a particular height in phase j; and δ, the fraction of the bed volume occupied by the bubbles, is given by [Kunii and Levenspiel, 1991],

$$\delta=\begin{cases}\dfrac{U_0-U_{mf}}{U_b+U_{mf}} & \text{when} \quad U_b\cong\dfrac{U_{mf}}{\varepsilon_{mf}}\\[2ex] \dfrac{U_0-U_{mf}}{U_b} & \text{when} \quad U_b\cong 5\dfrac{U_{mf}}{\varepsilon_{mf}}\end{cases} \tag{17}$$

The rate expression for the chlorination of rutile was experimentally determined as follows [Sohn et al., 1998]:

$$\frac{dr}{dt}=-k_v(RT)^{1.29}C_{co}^{0.55}C_{Cl_2}^{0.74}. \tag{18}$$

The mathematical model developed in this work considers the separate variations of the gas concentrations in the bubble and emulsion phases with bed height. With the assumption of steady state and perfect mixing of solid particles in the bed, an overall mass balance of the solid gives [Kunii and Levenspiel, 1968; Levenspiel et al., 1968]

$$F_0-F_1-F_2=\sum_{all\ r}\begin{pmatrix}\text{rate of solid consumption in}\\ \text{size interval r to r+dr}\\ \text{in the whole bed}\end{pmatrix} \tag{19}$$

and

$$\begin{pmatrix}\text{Rate of mass consumption}\\ \text{in the size interval r to}\\ \text{r+dr per unit}\\ \text{volume of the bed}\end{pmatrix}=\begin{pmatrix}\text{rate of mass consumption}\\ \text{in the size interval r to}\\ \text{r+dr in bubble phase}\\ \text{per unit volume of the bed}\end{pmatrix}+\begin{pmatrix}\text{rate of mass consumption}\\ \text{in the size interval r to}\\ \text{r+dr in emulsion phase}\\ \text{per unit volume of the bed}\end{pmatrix}. \tag{20}$$

In the bubble phase,

$$\begin{pmatrix}\text{Rate of mass consumption}\\ \text{in the size interval r to}\\ \text{r+dr in bubble phase}\\ \text{per unit volume of the bed}\end{pmatrix}=\rho\begin{pmatrix}\text{number of particles in}\\ \text{the interval r to r+dr}\\ \text{in bubble phase per}\\ \text{unit volume of the bed}\end{pmatrix}\times\begin{pmatrix}\text{rate of volume}\\ \text{decrease for}\\ \text{one particle in}\\ \text{bubble phase}\end{pmatrix}=\rho\left(\frac{y_b w P_1(r)dr}{\rho\left(\frac{4}{3}\pi r^3\right)}\frac{dV}{dt}\right) \tag{21}$$

A similar equation is written for the emulsion phase. In the preceding equations, F_0 is the feed rate of solids with a particle-size density function of $P_0(r)$; F_1 is the withdrawal rate of solids with a particle-size density function of $P_1(r)$; F_2 is the elutriation rate of solids with a particle-size density function of $P_2(r)$; ρ is the mass density of solid; y_b is the fraction of the entire solid present in the bubble phase; w is the solid weight per unit volume of the bed; r is the particle radius; and V is the volume of a particle.

The mass balance of solid in the particle-size interval r to r+dr in terms of rate gives,

$$\begin{pmatrix}\text{Solids}\\ \text{entering in}\\ \text{the feed}\end{pmatrix}-\begin{pmatrix}\text{solids}\\ \text{leaving in}\\ \text{overflow}\end{pmatrix}-\begin{pmatrix}\text{solids}\\ \text{leaving in}\\ \text{carryover}\end{pmatrix}+\left[\begin{pmatrix}\text{solids shrinking}\\ \text{into the}\\ \text{interval from}\\ \text{a larger size}\end{pmatrix}-\begin{pmatrix}\text{solids shrinking}\\ \text{out of the}\\ \text{interval to}\\ \text{a smaller size}\end{pmatrix}\right]-\begin{pmatrix}\text{solids consumption}\\ \text{due to the}\\ \text{shrinkage within}\\ \text{the interval}\end{pmatrix}=0. \tag{22}$$

The formulation of the quantitative expressions of the various terms in the above conceptual balance equations is described elsewhere [Zhou and Sohn, 1996]. The resulting model equations were applied to the cases of single-sized and multi-sized feeds.

To verify the mathematical model, batch experiments were carried out using a deep bed across which significant changes in gas concentrations occurred. Since the gas-phase dynamics are much faster than changes in the solid particles, the steady-state model was applied to each time increment, yielding the solid-particle-size distribution and the amount of solids remaining in the bed at various time increments. This is equivalent to the familiar pseudo-steady-state approximation applied to the analysis of gas-solid reactions [Szekely et al., 1976]. This was done because it is difficult to establish a true steady-state chlorination condition in a small laboratory apparatus with a small solid feed rate. An attempt to conduct the experiment in a true steady-state, continuous condition would only have introduced additional uncertainties and accompanying errors.

The most important variables affecting the performance of the bed and the reaction rate are superficial gas velocity and the exchange rate of gases between phases. In general, both chemical and hydrodynamic factors should be considered in elucidating the reactor performance [Grace, 1974; Chavarice and Grace, 1975; Fryer and Potter, 1975]. The mathematical model was tested by comparing the computed results with the results of experiments under carefully selected conditions in which both the chlorination kinetics and mass-transfer effects play a significant role. This way, generally valid verification of the model can be obtained.

Examples of the model predictions compared with the experimental results are shown in Fig. 19 for a feed with a wide size distribution. It is seen that the mathematical model yields results that are in good agreement in terms of overall conversion vs. time. The calculated results of the particle size distributions in the bed and in the elutriation are given in Fig. 20. This work represents another example of the application of chemical reaction engineering principles to the quantitative analysis of a rather complex system involving the chemical processing of inorganic materials.

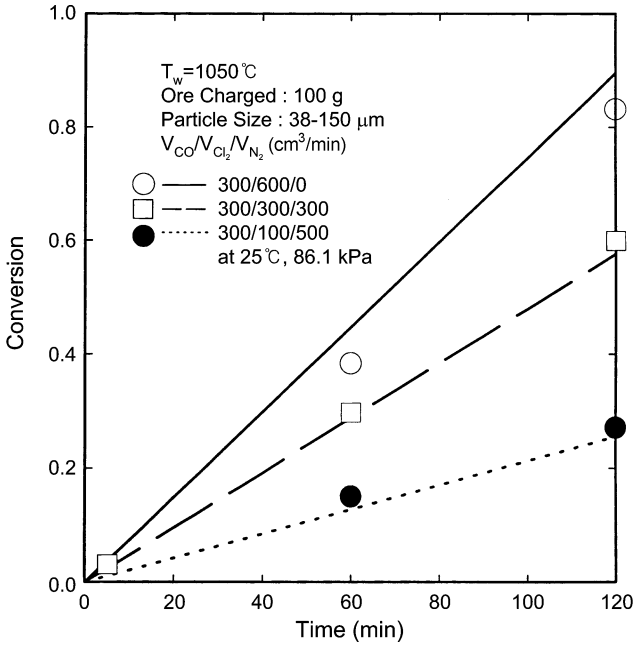

Fig. 19. Experimental data vs. model prediction for the fluidized-bed chlorination of rutile particles with a wide size distribution (The feed particle size distribution can be found in Fig. 20).

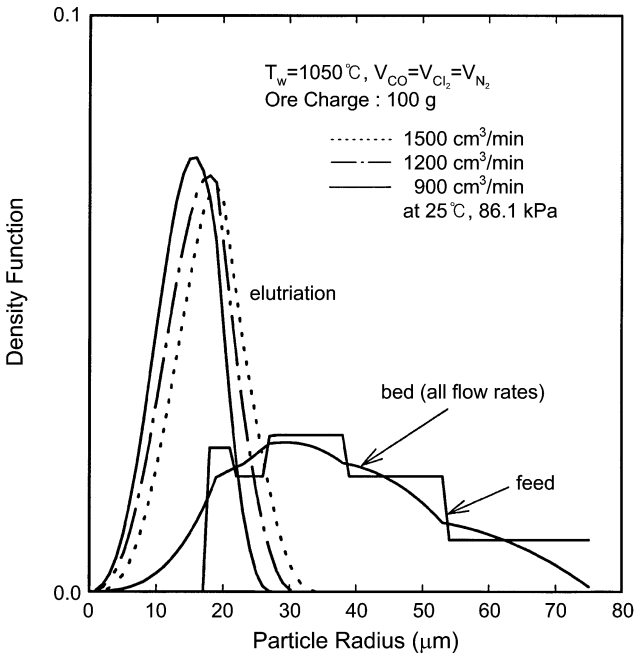

Fig. 20. Computed particle-size density function in the bed and elutriation for the fluidized-bed chlorination of rutile particles with a wide size distribution.

CLOSING REMARKS

Several examples have been discussed in this article that illustrate the application of chemical reaction engineering principles to the modeling and analysis of complex systems involving the chemical processing of metals and inorganic materials. The rapidly increasing computational capacity enables us to simulate these complex systems with increasing accuracies, incorporating greater realistic details.

It is further noted that this ability to simulate complex systems in greater details specific to each system will result in the merging of many sub-disciplines of chemical engineering. The separate treatments of individual aspects, such as fluid flow, reaction rates, and heat/mass transfer, in a complex process will be replaced to an increasing extent by more realistic and detailed quantitative analysis by means of mathematical formulations that simultaneously incorporate a combination of the appropriate sub-disciplines.

ACKNOWLEDGMENTS

I wish to acknowledge the contributions of my present and former graduate students and research associates, many of whom are Koreans, for making it possible to obtain fruitful research results. Many colleagues in the professional community have also provided valuable ideas and helpful discussions on various aspects of the work described in this article. Numerous public agencies and private companies, individually acknowledged in the papers referenced in this article, have financially supported our research work over the years, for which I am grateful.

REFERENCES

Alegret, S. (ed.), "Developments in Solvent Extraction," Ellis Horwood Ltd. (1988).

Batey, W., Arthur, T., Thompson, P. J. and Thornton, J. D., "The Dynamics of Pulsed Plate Extraction Columns," in Ref. 24, pp. 166-167.

Blumberg, R., "Liquid-Liquid Extraction," Academic Press (1988).

Burkur, D. B., Wittmana, C. V. and Amundson, N. R., "Analysis of a Model for a Nonisothernal Continuous Fluidized Bed Catalytic Reactor," *Chem. Eng. Sci*., **29**, 1173 (1974).

Chaubal, P. C., "The Reaction of Chalcopyrite Concentrate Particles in a Flash Furnace Shaft," Ph. D. Dissertation, University of Utah, Salt Lake City, Utah, U. S. A. (1986).

Chaubal, P. C. and Sohn, H. Y., "Intrinsic Kinetics of the Oxidation of Chalcopyrite Particles under Isothermal and Non-Isothermal Conditions," *Metall. Trans. B*, **17B**, 51 (1986).

Chavarice, C. and Grace, J. R., "Performance Analysis of a Fluidized Bed Reactor," *Ind. Eng. Chem. Fund*., **14**, 75 (1975).

Clift, R. and Clift, J. R., "Continuous Bubbling and Slugging," Chap. 3 in Fluidization, 2nd ed., by J. F. Davidson, R. Clift, and D. Harrison, Academic Press, Orlande, Florida, 73 (1985).

Davidson, J. F., Harrison, D., Darton, R. C. and LaNauze, R. D., Chap. 10 in Chemical Reactor Theory, A Review, ed. by L. Lapidus and N. R. Amundson, Prentice Hall, Englewood Cliffs, New Jersey, 583 (1977).

Drinkenburg, A. A. H. and Rieteura, K., "Gas Transfer from Bubble in a Fluidized Bed to the Dense Phase," *Chem. Eng. Sci*., **27**, 1765 (1972).

Extraction '84, The Institution of Chem. Engrs. Symp. Ser. No. 88 (1984).

Fei, W.-Y. and Slater, M. J., "A New Look at the Hydrodynamic Behavior of Rotating Disc Contactors," International Solvent Extraction Conference (ISEC) '83, American Institute of Chemical Engineers, New York, 174 (1983).

Fryer, C. C. and Potter, O. E., "Experimental Investigation of Models for Fluidized Bed Catalytic Reactors," *AIChE J*., **22**, 38 (1975).

Fuwa, A., Kimura, E. and Fukushima, S., "Kinetics of Iron Chlorination of Roasted Ilmenite Ore, Fe_2TiO_5 in a Fluidized Bed," *Metall. Trans. B*, **9B**, 643 (1978).

Garg, M. O. and Pratt, H. R. C., "Steady-State Droplet Size Distribution in a Pulsed Plate Extraction Column," in International Solvent Extraction Conference (ISEC) '83, American Institute of Chemical Engineers, New York, 157 (1983).

Grace, J. R., "Fluidization and its Application to Coal Treatment and Applied Processes," in Fluidization and Fluid-Particle Systems, AIChE Symp. Ser., Vol. 70, No. 141, American Institute of Chemical Engineers, New York, 21 (1974).

Hahn, Y. B. and Sohn, H. Y., "Mathematical Modeling of Sulfide Flash Smelting Process: Part I. Model Development and Verification with Laboratory and Pilot-Plant Measurements for Chalcopyrite Concentrate Smelting," *Metall. Trans. B*, **21B**, 945 (1990).

Husung, G., Gaubinger, W. and Marr, R., "Drop Size, Specific Agitation Power and Energy Dissipation for Countercurrent Extraction Columns," International Solvent Extraction Conference (ISEC) '83, American Institute of Chemical Engineers, New York, 52 (1983).

Itagaki, K., Sohn, H. Y. and Pérez-Tello, M., "Basic Principles of Sulfide Smelting and Converting with Oxygen-Rich Gas," Sulfide Smelting 2002, ed. by R. L. Stephens and H. Y. Sohn, TMS, Warrendale, Pennsylvania, 15 (2002).

Iyer, K. M. and Sohn, H. Y., "Backmixing in Channel Reactors with High-Strength Bottom Gas Injection," *Metall. Mater. Trans. B*, **25B**, 619 (1994).

Iyer, K. M. and Sohn, H. Y., "Mass Transfer Analysis for Pyrometallurgical Channel Reactors with High-Strength Bottom Gas Injection," in Extractive Metallurgy of Copper, Nickel and Cobalt, Vol. 1. Fundamental Aspects, edited by R. G. Reddy and R. N. Weizenbach, TMS, Warrendale, Pennsylvania, 223 (1993).

Iyer, K. M. and Sohn, H. Y., "Physical and Mathematical Modeling of Pyrometallurgical Channel Reactors with Bottom Gas Injection: Residence Time Distribution Analysis and Ideal-Reactor-Network Model," *Metall. Mater. Trans. B*, **25B**, 207 (1994).

Jackson, E., "Hydrometallurgical Extraction and Reclamation," Ellis Horwood, Ltd. (1986).

Kato, K. and Wen, C. Y., "Bubble Assemblage Model for Fluidized Bed Catalytic Reactors," *Chem. Eng. Sci*., **24**, 1351 (1969).

Kunii, D. and Levenspiel, O., "Fluidization Engineering," Wiley, New York (1991).

Kunii, D. and Levenspiel, O., "Bubbling Bed Model for Kinetic Process in Fluidized Beds. Gas-solid Mass and Heat Transfer and Catalytic Reactions," *Ind. Eng. Chem., Process Des. Develop*., **7**, 481 (1968).

Laddha, G. S. and Degaleesan, T. E., "Transport Phenomena in Liquid Extraction," McGraw-Hill, 213 (1978).

Laddha, G. S. and Degaleesan, T. E., "Dispersion and Coalescence," in "Handbook of Solvent Extraction," ed. by T. C. Lo, M. H. I. Baird and C. Hanson, Wiley, New York, 125 (1983).

Lee, M. S. and Sohn, H. Y., "Dispersed-Phase Holdup in Liquid-Liquid Emulsions Generated by High-Strength Bottom Gas Injection," *Metall. Mater. Trans. B*, **27B**, 213 (1996).

Lee, Y. K. and Kim, C., "A Study on the Drop Size Distribution and the Holdup in a Rotating Impeller Extraction Column," in Solvent Extraction 1990, ed. by T. Sekine, Elsevier, Amsterdam, 1253 (1992).

Levenspiel, O., Chemical Reaction Engineering, 3rd ed., Wiley, New York (1999).

Levenspiel, O., Kunii, D. and Fitzgerald, T., "The Processing of Solids of Changing Size in Bubbling Fluidized Beds," *Powder Technol*., **2**, 87 (1968).

Lo, T. C., Baird, M. H. I. and Hanson, C. (eds.), "Handbook of Solvent Extraction," Wiley (1983).

Nyman, B., Yllö, E. and Lantto, T., "Innovative Copper Recovery by Outokumpu's VSF Technology," in Copper 95, Vol. III - Electrorefining and Hydrometallurgy of Copper, ed. by W. C. Cooper et al., CIM, Montreal, 605 (1995).

Perez-Tello, M., Sohn, H. Y. and Smith, P. J., "Experimental Investigation and 3-D Computational Fluid Dynamics Modeling of the Flash Converting Furnace Shaft: Part II. Formulation of 3-D Computational Fluid Dynamics Model Incorporating the Particle Cloud Description," *Metall. Mater. Trans. B*, **32B**, 869 (2001).

Perez-Tello, M., Sohn, H. Y., St. Marie, K. and Jokilaakso, A., "Experimental Investigation and 3-D Computational Fluid Dynamics Modeling of the Flash Converting Furnace Shaft: Part I. Experimental Observation of Copper Converting Reactions in Terms of Converting Rate, Converting Quality, Changes in Particle Size, Morphology, and Mineralogy," *Metall. Mater. Trans. B*, **32B**, 847 (2001).

Pyle, D. L., "Fluidized Bed Reactors: A Review," in Chemical Reaction Engineering, Advances in Chemistry Series 109, ed. by R. F. Gould, American Chemical Society, Washington DC, 106 (1972).

Rauscher, H. and Blass, E., "Operation of a Pulsed Sieve-Plate Extraction Column with an Extreme Phase Flow Ratio," in Solvent Extraction 1990, ed. by T. Sekine, Elsevier, Amsterdam, 1271 (1992).

Rhee, K. I. and Sohn, H. Y., "The Selective Chlorination of Iron from Ilmenite Ore by CO-Cl_2 Mixtures: Part II. Mathematical Modeling of Fluidized-Bed Process," *Metall. Trans. B*, **21B**, 331 (1990).

Ricci, L. (ed.), "Separation Techniques: I. Liquid-Liquid Systems," Chemical Engineering McGraw Hill Pub. Co. (1980).

Schmidt, H., "Holdup, Drop Size and Axial Mixing of Pulsed Extraction Columns," *ibid.*, pp. 164-165.

Schulte, L. D., Los Alamos National Laboratory, personal communication (1998).

Seo, K. W. and Sohn, H. Y., "Mathematical Modeling of Sulfide Flash Smelting Process: Part III. Volatilization of Minor Elements," *Metall. Trans. B*, **22B**, 791 (1991).

Simons, A. J. F. and Nap, C., "Dynamic Simulation of Pulsed Packed Columns," in International Solvent Extraction Conference (ISEC) '83, American Institute of Chemical Engineers, New York, 209 (1983).

Simons, A. J. F., "Pulsed Packed Columns," in Handbook of Solvent Extraction, ed. by T. C. Lo, M. H. I. Baird, and C. Hanson, Wiley, New York, 343 (1983).

Sohn, H. Y. and Doungdeethaveeratana, D., "A Novel Extraction Process with Bottom Gas Injection without Moving Parts," *Separation and Purification Technol.*, **13**, 227 (1998).

Sohn, H. Y. and Seo, K. W., "Flash Combustion of Sulfide Mineral Particles in a Turbulent Gas Jet," in Multiphase Transport and Particulate Phenomena, Vol. 3, edited by T. N. Veziroglu, Proceedings of the 5th Miami International Symposium on Multi-Phase Transport and Particulate Phenomena, December 12-14, 1988, Miami Beach, Florida, Hemisphere Publishing Corp., New York, 501 (1990).

Sohn, H. Y., Seo, K. W., Chaubal, P. C. and Hahn, Y. B., "Laboratory Studies on the Flash Smelting of Copper Concentrate," in Flash Reaction Processes, Proceedings of the 1988 Center for Pyrometallurgy Conference, Salt Lake City, Utah, June 15-17, 1988, edited by D. G. C. Robertson, H. Y. Sohn, and N. J. Themelis, published by the Center for Pyrometallurgy, University of Missouri-Rolla, Rolla, Missouri, 145 (1988).

Sohn, H. Y., Zhou, L. and Cho, K., "Intrinsic Kinetics and Mechanism of Rutile Chlorination by CO+Cl_2 Mixtures," *Ind. Eng. Chem. Research*, **37**, 3800 (1998).

Stoller, S. M. and Richards, R. B. (eds.), "Reactor Handbook, Vol. II, Fuel Reprocessing," Interscience, New York (1961).

Szekely, J., Evans, J. W. and Sohn, H. Y., "Gas-Solid Reactions," Academic Press, New York (1976).

Van Swaaij, W. P. M. and Zuiderweg, F. J., "Investigation of Ozone Decomposition in Fluidized Bed on the Basis of a Two Phase Model," *Chem. React. Eng., Proc. Eur. Symp.*, **B9**, 25 (1972).

Werther, J., "Scale-up of Fluidized Bed Reactors," *Ger. Chem. Eng.*, **1**, 243 (1978).

Yasuda, Y. and Sohn, H. Y., "Experimental and Theoretical Study of Particle Dispersion Phenomena in a Turbulent Gas Jet of the Flash-Smelting Process by the Image Analysis Technique," *Metall. Mater. Trans. B*, **26B**, 637 (1995).

Youn, I.-J. and Park, K. Y., "Modeling of Fluidized Bed Chlorination of Rutile," *Metall. Trans. B*, **20B**, 959 (1989).

Zaidi, A. and Sohn, H. Y., "Measurement and Correlation of Drop-Size Distribution in Liquid-Liquid Emulsions Formed by High-Velocity Bottom-Gas Injection," *ISIJ International*, **35**, 234 (1995).

Zhou, L. and Sohn, H. Y., "Mathematical Modeling of Fluidized Bed Chlorination of Rutile," *AIChE J.*, **42**, 3102 (1996).

Zhu, F. G., Ni, X. D. and Su, Y. F., "A Modified Rotating Disk Contactor with Wire Mesh Coalescers," International Solvent Extraction Conference (ISEC) '83, American Institute of Chemical Engineers, New York, 143 (1983).